A structure-coupled CFD method for time-marching flutter analysis

N. V. Taylor, C. B. Allen, A. Gaitonde and D. P. Jones
University of Bristol, UK

ABSTRACT

Aeroelastic analysis is a critical area of the aircraft design process, as a good understanding of the dynamic behaviour of the wing structure is essential to safe operation of the vehicle. The inevitable inaccuracies present in the modelling of such phenomena impose mass penalties, as large safety margins are necessitated, which in turn lead to overly stiff designs. In an effort to reduce the uncertainty in analysis methods, fully coupled CFD and structural models are under widespread development. This paper describes the results produced by such a system for a series of test cases based on the AGARD445.6 and MDO wings. Results relating to the latter are of particular interest, as significant variations were found to be produced by the different methodologies used in previous studies, the precise cause of which could not be isolated. In an effort to provide this isolation, a detailed description of the method used is given, including the interpolation scheme between the structural model and the aerodynamic surface, and particular attention is given to the issue of aerofoil shape preservation.

NOMENCLATURE

a	speed of sound, stiffness damping coefficient
b	mass damping coefficient
c_r	root chord
$\mathbf{C}$	damping matrix
C_L	lift coefficient
$\mathbf{E}$	matrix of mode vectors, Young's Modulus
f	frequency
F	force
$\mathbf{K}$	stiffness matrix
$\mathbf{m}$	modal unit displacement vector in Cartesian space, mass
$\mathbf{M}$	mass matrix, Mach number
P	pressure
t	time
T	temperature
$\mathbf{u}$	modal displacement vector in Cartesian space
U	velocity
U^*	flutter speed index
$\mathbf{x}$	modal position vector
X,Y,Z	Cartesian co-ordinates
$\bar{\alpha}, \bar{\delta}$	Newmark parameters
μ	mass ratio
ν	Poisson ratio, truncated cone volume
ρ	density
ω	mode frequency
ζ	damping ratio

Subscripts

m	modal
e	external
∞	freestream conditions

Superscripts

i	mode number index

1.0 INTRODUCTION

The prediction and analysis of the aeroelastic behaviour of an aircraft is of critical importance, as any unstable response to time varying or impulsive loads (gusts, etc.) may rapidly lead to disastrous structural failure. This danger requires significant safety margins, proportionate to the level of inaccuracy and uncertainty inherent in the prediction method used. This increased safety margin results in unnecessary stiffness, and hence a higher structural weight.

Methods currently common for aeroelastic analysis in industry involve the use of linear techniques for both flutter and aeroservoe-

Paper No. 2885. Manuscript received 15 March 2004, revised version received 16 June 2004, accepted 22 June 2004.

https://doi.org/10.1017/S0001924000000208 Published online by Cambridge University Press

lastic problems, allowing uncoupling of the aerodynamic and structural equations. This reduces the accuracy of the methods, particularly in the transonic region of flight regime where the aerofoil thickness (usually neglected) plays a crucial role in the development and movement of shock waves. They are also inapplicable to non-linear instabilities such as control surface buzz and limit cycle oscillation.

A new approach is therefore under widespread development, consisting of simulation by non-linear CFD analysis coupled to a dynamic structural representation of the body under investigation[1-14]. This allows non-linear analysis of dynamic behaviour in the time domain, leading to much more accurate methods for flutter investigation. This paper describes the results produced by a moving mesh, unsteady, implicit, cell centred finite volume code when coupled to linear modal analysis, for two widely used test cases, specifically the AGARD445.6 and MDO wings.

The latter case in particular is of interest, as previous work identified significant differences in pressure distribution and dynamic behaviour between various coupled methods, without identifying the specific cause[15,16]. Possible explanations for these differences were given, being the accuracy with which the CFD scheme calculates the loading, the effectiveness and consistency of the load transfer algorithm, the accuracy of the structural calculation, and the accuracy with which the displacement algorithm transforms the aerodynamic shape (Ref. 15, page 318). In order to isolate the impact of each of these effects, a full description of the interpolation scheme is given, and particular attention is given to aerodynamic interpolation and examining the impact of solution differences on the results, where significant.

2.0 COUPLED CODE

The CFD scheme used as the basis for this work was USCRANSMB. This is a derivative of BAE Systems' code RANSMB, a cell centred solver based on the Jameson method[17,18]. Work at the University of Bristol has extended the code to allow fully implicit unsteady calculations for structure coupled analysis through a pseudo time stepping method[19-21], and a moving mesh sprung block system. It has previously been shown that little effect on flutter boundary prediction is produced by the inclusion of viscous effects[22-25], and hence only the Euler equations were solved. The aerodynamic grids were supplied by Glasgow University, and converted to USCRANSMB format.

2.1 Time integration scheme

The structural model consisted of the mode shapes and frequencies produced by a NASTRAN based analysis of the wing structure. Once read in to the coupled code, the modal force associated with mode i is calculated from

$$F_m^i = F_e . m^i \qquad \ldots (1)$$

where F_e is the force applied externally at each node, and m^i the ith mode shape vector non-dimensionalised with respect to mass. As the CFD solution is coupled to the structure by strong coupling[26,27], F_e is the predicted force at time step $t + \Delta t$. Whilst the structural damping present in the test cases under consideration is not modelled, in the case of the AGARD445.6 wing because it is small and difficult to quantify, and for the MDO because this structure is entirely computationally derived and has no damping, the test cases associated with the MDO wing require excitation from an equilibrium steady state wing position which is itself distorted from the nominal jig shape. In order to obtain this distorted position under atmospheric conditions beyond the stability boundary, artificial damping must be applied to the system, which is then removed before the dynamic motion is initiated. The ability to include an arbitrary level of damping into the system also allows more rapid attainment of steady state deflections under stable flow conditions. The motion of the system is therefore described by

$$\ddot{x} + [2\omega\zeta]\dot{x} + [\omega^2]x = F_m \qquad \ldots (2)$$

where ω^2 is a diagonal matrix made up of the square of the frequency of each mode, ζ is the damping ratio, and F_m is the vector of modal forces. The damping matrix, [**C**] is defined following Ref. 28 by

$$[\mathbf{C}] = a[\mathbf{K}] + b[\mathbf{M}] \qquad \ldots (3)$$

The values of a and b may either be selected to best represent the damping behaviour of a real wing or, if artificial damping is intended, selected to achieve desired damping characteristics by prescribing the result of the formula for each modal damping coefficient, given by

$$\zeta_i = \frac{1}{2}\left(a\omega_0^i + \frac{b}{\omega_0^i}\right) \qquad \ldots (4)$$

Equation (2) may be integrated forward in time using the Newmark scheme[29]:

$$\dot{x}^{t+\Delta t} = \dot{x}^t + \Delta t\left(1-\bar{\delta}\right)\ddot{x}^t + \Delta t\bar{\delta}\ddot{x}^{t+\Delta t} \qquad \ldots (5)$$

$$x^{t+\Delta t} = x^t + \Delta t\dot{x}^t + \Delta t^2\left(\frac{1}{2}-\bar{\alpha}\right)\ddot{x}^t + \Delta t^2\bar{\alpha}\ddot{x}^{t+\Delta t} \qquad \ldots (6)$$

where $\bar{\alpha}$ and $\bar{\delta}$ are set to their usual (unconditionally stable) values of 0·5 and 0·25 respectively. Substituting these values into Equation (2) gives

$$\left[[\mathbf{I}] + \Delta t\bar{\delta}[2\omega\zeta] + \Delta t^2\bar{\alpha}[\omega^2]\right]\ddot{x}^{t+\Delta t} = F_m - [\omega^2]\left(x^t + \Delta t\dot{x}^t + \left(\frac{1}{2}-\bar{\alpha}\right)\Delta t^2\ddot{x}^t\right) - [\mathbf{C}]\left(\dot{x}^t + \Delta t\left(1-\bar{\delta}\right)\ddot{x}^t\right) \qquad \ldots (7)$$

where [**I**] is the identity matrix. Assuming a known initial state, the entire right hand side of Equation (7) is known, and as [**I**], [2 $\omega\zeta$], and [ω^2] are known and diagonal, the solution of this equation may be obtained directly. Substitution then allows calculation of $\dot{x}$ and x.

Once the modal displacement is calculated, the Cartesian displacement at each node follows from

$$u = [\mathbf{E}]x \qquad \ldots (8)$$

where [**E**] is the matrix of mode vectors[26]. This deformed structural mesh is used to generate an aerodynamic surface through the interpolation scheme discussed in the following section. The flow about this new surface is calculated through a specified number of pseudo time steps to achieve convergence, completing the coupled cycle. The pressure distribution thus calculated may then be used to re-estimate f_m and a new coupling cycle initiated, or if a sufficient number at time t are complete, real time is incremented.

2.2 Interpolation scheme

The interpolation of the displacements from the structural grid to the aerodynamic grid is a two stage process. The method used here introduces an intermediate grid in an attempt to overcome the problems associated with structural and aerodynamic grids which do not occupy the same physical space. Unlike the virtual surface method[30-32] which also uses an intermediate surface between the CFD and FE meshes, in this case the intermediate grid is defined by the intersection of the structural surface normals with the aerody-

https://doi.org/10.1017/S0001924000000208 Published online by Cambridge University Press

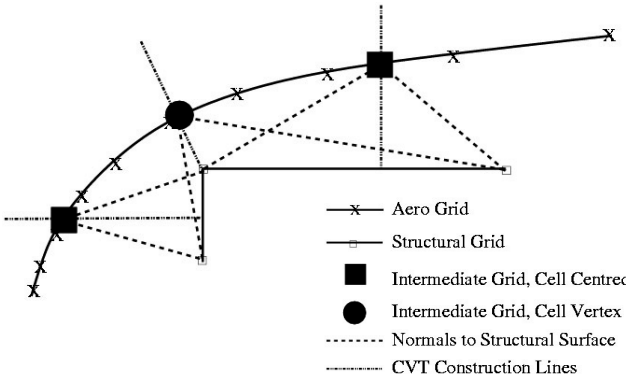


Figure 1. Relationship between structural, interpolated, and aerodynamic grids.

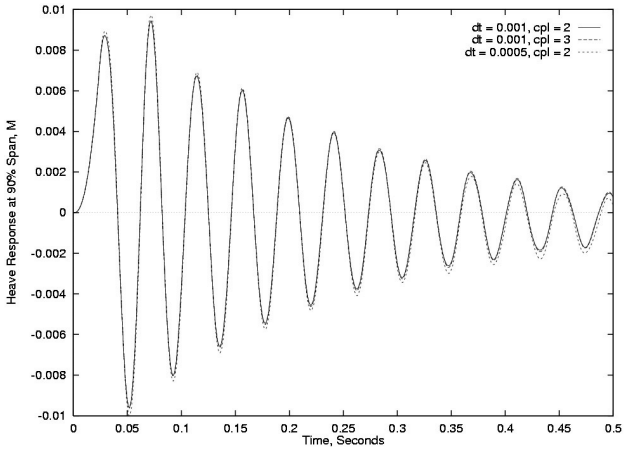


Figure 2. Effect of coupled cycles and time step M = 1·141, U^{*1} = 0·56.

Table 1
Modal frequencies of the AGARG445.6 wing

Model	Mode 1	Mode 2	Mode 3	Mode 4
Measured (Yates *et al*)[42]	9·60	38·10	50·70	98·50
Lee and Batina[11]	9·60	38·17	48·35	91·54
Goura *et al*[8]	9·67	36·87	50·26	90·00
Bristol	9·40	39·55	48·87	94·42

namic surface (see Fig. 1). The FE surface mesh is decomposed into triangular elements, and structural surface normals can be taken from the centres of these and/or the FE node points. The interpolation of displacements, from the structure, onto this intermediate surface is accomplished via the constant volume tetrahedra (CVT) transformation[33,34].

The interpolation of the displacements from the intermediate surface to the aerodynamic grid is now significantly simplified as the surfaces coincide. The transformation method used in this case is the thin plate spline[35-38]. Investigations showed that the thin plate spline worked very well on aerofoil type structures as long as points at the leading and trailing edges are included in the intermediate grid[39]. A detailed description and analysis of the method of transformation is given in Ref. 40.

The force transformation from the aerodynamic to structural grid uses the virtual work principle[34,37,39]. Effectively, the transpose of the displacement transformation matrix becomes the force transformation. Once again this uses the intermediate grid as this is more efficient in storage and calculation time.

3.0 THE AGARD445.6 WING

The AGARD445.6 is a tapered wing swept at 45° at the quarter chord. It has root and tip chords of 0·558m and 0·368m, and a semi span of 0·762m. The section is a NACA 65A004 aerofoil, and is hence symmetric with a maximum thickness of 4% of the local chord. The wing was modelled in NASTRAN using CQUAD4 elements with local aerofoil thickness at each node and properties of E_1 = 3·151*10^9 NM^{-2}, E_2 = 4·162*10^8 NM^{-2}, ν_{12} = 0·31, and a density of 381·98 kgM^{-3}. Nodes were placed on lines parallel to the root chord with constant spanwise spacing. Distribution in the chordwise direction was also constant as a proportion of the local chord. The grid covered the entire planform of the wing, and contained 11 equidistant nodes in span and local chord directions. The number of modes extracted was limited to four, to match the models used in Refs 8, 11 and 41. The frequencies of these modes compare well with these other sources, as shown in Table 1.

As the AGARD445.6 wing is symmetrical and of low mass, at zero incidence no spanwise deflections would be expected at any flow speed. This means that the flow field produced by uncoupled solution may be used as an initial steady state condition for the coupled solver. The wing is then set in motion, and its response in the time domain computed.

The non-dimensional velocity of the flow was calculated from

$$U^* = \frac{U_\infty}{\frac{1}{2} c_r \omega_\alpha \sqrt{\mu}} \quad \ldots (9)$$

where U_∞ is the freestream velocity, c_r the root chord, ω_α the frequency of the first torsional mode (the second mode in Table 1, and hence equal to 39·55Hz), and μ is the mass ratio, given by

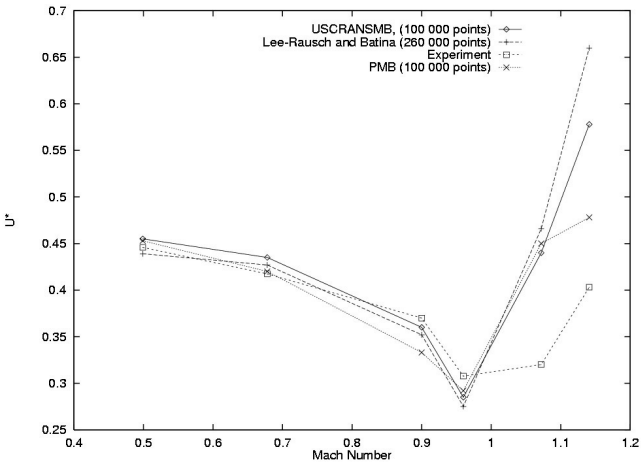
$$\mu = \frac{m}{\rho_\infty \nu} \quad \ldots (10)$$

where ρ_∞ is freestream density, the mass of the wing (m) is 1·836kg[8], and ν, the volume of the truncated cone surrounding the wing with diameter equal to local chord, is 0·130m^3 [8,43]

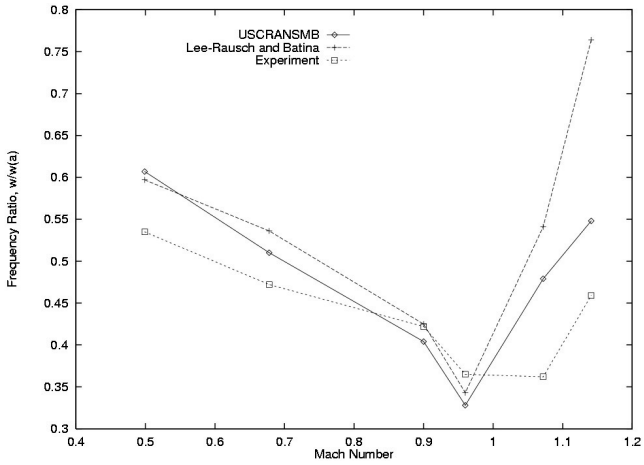
The upstream speed of sound (a_∞) was held at a constant value of 320ms^{-1}. Mach numbers were chosen to match the experimental values, and this in turn defined U_∞. It may be shown that U^* is a function of Mach number and freestream pressure only for a given wing[44], and hence only the free stream pressure may be used to vary U^* in order to locate U^*_{crit}, the flutter velocity for a given Mach number. The heave and pitch response of the wing at 90% span at several values of free stream pressure were analysed, and the percentage by which the magnitude of the final oscillations were above or below the average over the entire calculation found. This allowed interpolation to be used to locate the value of U^* at which the response was neither growing nor decaying, defined as the flutter boundary.

The aerodynamic grid supplied by Glasgow University consisted of approximately 100,000 points in eight blocks. Initially, the real time step was set to 0·001 seconds (50 points per cycle at a nominal flutter frequency of 20Hz), and two coupling cycles of 10 pseudo iterations were used at each real time step. To examine the convergence of the computational scheme, the time step was then halved, and, independently, the number of coupling cycles at each time step was increased to three. Results for a Mach number of 1·141 (that most affected) are presented in Fig. 2. As may be seen, the effect of both of these

https://doi.org/10.1017/S0001924000000208 Published online by Cambridge University Press



(a) flutter boundary



(b) flutter frequency ratio

Figure 3. Comparison of various AGARD445.6 flutter results.

changes is negligible, and hence the initial scheme may be considered to be converged with respect to these variables. These parameters were thus used for all further calculations for the AGARD445.6 wing. A typical run comprising 500 real time steps (i.e. 0·5 seconds of response) required approximately 10 hours on a 500 MHz. EV6 Compaq Alpha server.

Figure 3(a) shows a comparison between the flutter boundary located by the current method, and various other coupled CFD-modal solution methods. Agreement is generally good across the entire Mach number range. Although at high Mach numbers correlation with the experimental results does deteriorate, this is a feature of all the coupled calculations. The frequency at which flutter occurs is shown in Fig. 3(b) (relative to that of the first torsional mode). Again agreement between available experimental and computational results is generally good, although experimental and theoretical results diverge in the supersonic region.

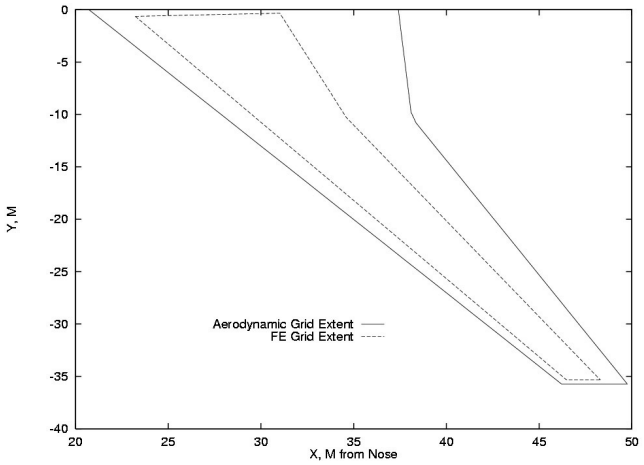


Figure 4. Aerodynamic and structural grid sizes of the MDO wing.

4.0 THE MDO WING

The MDO (multi-disciplinary optimisation) vehicle was designed in a Brite-Euram project explicitly to investigate optimisation methods useful for the design of next-generation large transport aircraft. The highly flexible wing may be extracted from the complete aircraft model, and used for unsteady calculations. This was achieved by the partners in the Unsteady Flow in the Context of Fluid-Structure Interaction (UNSI) project (a summary of results appears in Refs 15 and 16. Similar work has also been undertaken at Glasgow University[45], who again provided an aerodynamic grid, and in this case also the structural modes. The MDO wing presents a more challenging test case for the coupled method than the AGARD445.6, due to the increased complexity of the wing aerodynamics and structure (being neither thin nor symmetrical).

4.1 Models and meshes

The semi-span of the MDO vehicle wing is approximately 36m, and has a planform as shown in Fig. 4. Also shown on this figure is a plan view of the structural grid, demonstrating that the MDO model wing box has a chord of only about half that of the local aerofoil. The structural model itself essentially consists of two plates, each nearly coincident with either the upper or lower wing surface. There are no nodes between these two plates through the aerofoil thickness, and hence the vertical walls of the wing box are formed from single elements. This mesh presents a greater challenge for the interpolation technique used to physically couple the structural and aerodynamic meshes, particularly for points near the leading or trailing edges.

The wing is of a thick supercritical section, and hence the variation from conventional linearised aerodynamic theory produced by the coupled Euler solver would be expected to be much greater than that for the AGARD445.6 wing. The aerodynamic grid supplied by Glasgow has approximately 106,000 points, and the structural model comprised 18 modal vectors on a grid containing 2,515 nodes, split between the upper and lower surfaces. There were 35 spanwise sections, each with between 36 and 8 nodes in chord (less at the tip). This produced a much finer mesh than that used for structural analysis of the AGARD445.6 wing, although limited in the chordwise extent, as noted previously.

4.2 UNSI test cases

The test cases investigated by the partners involved in UNSI consisted of three design point calculations. The static deflections produced in

https://doi.org/10.1017/S0001924000000208 Published online by Cambridge University Press

Table 2
MDO test cases: free stream properties

Case	M	C_L	Mass	Alt	T	P	ρ_∞	a_∞	U_∞
Units	-	-	tons	km	K	Pa	kgm^{-3}	ms^{-1}	ms^{-1}
1	0·85	0·4581	371	11·27	216·6	21,662	0·348	295·0	250·8
2	0·88	0·3263	537	7	242·7	41,060	0·5895	312·3	274·8
3	0·88	0·1686	537	2	275·2	79,495	1·007	332·5	292·6

the steady state were compared for all three, and the dynamic behaviour of cases two and three following an initial modal excitation were also examined. The cases are defined by a required lift coefficient rather than angle of attack, and are as given in Table 2. The lift coefficient calculated was referenced to the full 725m^2 wing area of the MDO aircraft, despite the fact that only the exposed portion of the wing was used in the calculations.

All three test cases are compared with available data at steady state conditions by allowing an initial flowfield produced by the uncoupled code to evolve into dynamic equilibrium between aerodynamic and structural forces. Damping was applied to each mode to reduce the time taken to achieve the steady state. The location of the leading and trailing edges of the wing could then be compared with available data, and aerofoil cross section distortion examined to determine the effectiveness of the interpolation scheme.

The flow field produced was then used to provide initial conditions for the unsteady flow calculations required for the dynamic behaviour produced by the aerodynamic conditions detailed by Cases 2 and 3. The wing motion was initiated by restarting the coupled solver (without damping) by applying an initial modal velocity in the first mode of

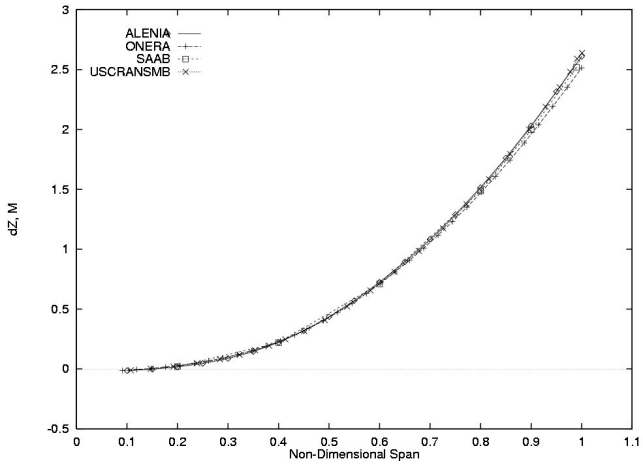
$$\dot{x}_0^{t=0} = 2\pi f_1 x_1 \qquad \ldots (11)$$

where f_1 is the first mode frequency, and x_1 is specified as the modal displacement which would result in a tip deflection of 1m.

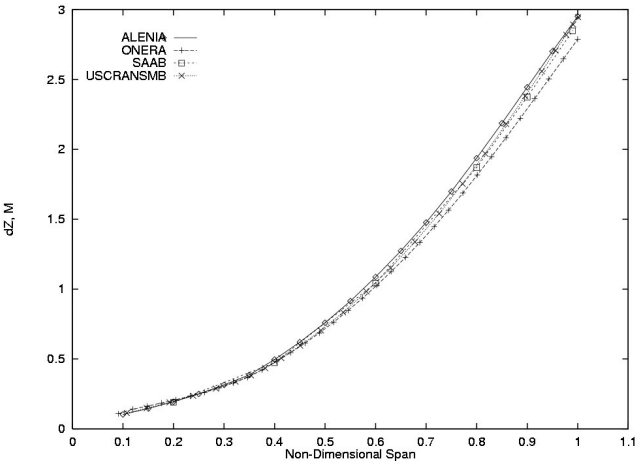
While a total of eight different solution methods were used by the UNSI partners, they varied from coupled Euler — NASTRAN to viscous full potential and transonic perturbation schemes coupled to modal analysis. Therefore, only the most similar to the Euler-Modal analysis of USCRANSMB have been included for comparison. These methods were: ONERA's structured cell-centred Euler solver (CANARI), using a NASTRAN-based 20-mode structural model to define structural motion for the transpiration-based aerodynamics; and SAAB's Euler solver (EURANUS), based upon a full second order spatial cell centred and upwind high-resolution scheme coupled to an 18-mode structural model with pre-generated modal perturbation meshes used to define mesh motion. The ONERA aerodynamic grid contained 365541 nodes, and the SAAB grid 106425. ALENIA also used an Euler solver (UES3D), although on an unstructured aerodynamic mesh coupled directly to MSC NASTRAN, using a mesh deformation technique. However, the majority of their calculations included the effect of gravity (in the present analysis ignored) and hence only in the first test case may their results be used for comparison. The pressure distributions and edge deflections were taken from the UNSI web page at *http://www.unsi.dlr.de/database*. For dynamic calculations, only the ONERA results were available for comparison (taken from the same website). The time step used by ONERA of 0·01 seconds was used for these dynamic calculations.

4.2.1 Case 1

The first test case, defined as 'economic cruise', required a lift coefficient of 0·4581. An incidence of 0·931 degrees produced a value of 0·4577, sufficiently close to that required. This incidence compares reasonably well with results from the other Euler-Modal coupled solutions produced by SAAB and ONERA of 0·745 and 0·8925 degrees respectively, although in less good agreement with the ALENIA result of 0·3002 (as discussed in Ref. 15, the discrepancy here is most likely caused by differences in structural model, ALENIA being the only group member to use a full FE rather than modal analysis).



(a) leading edge deformation



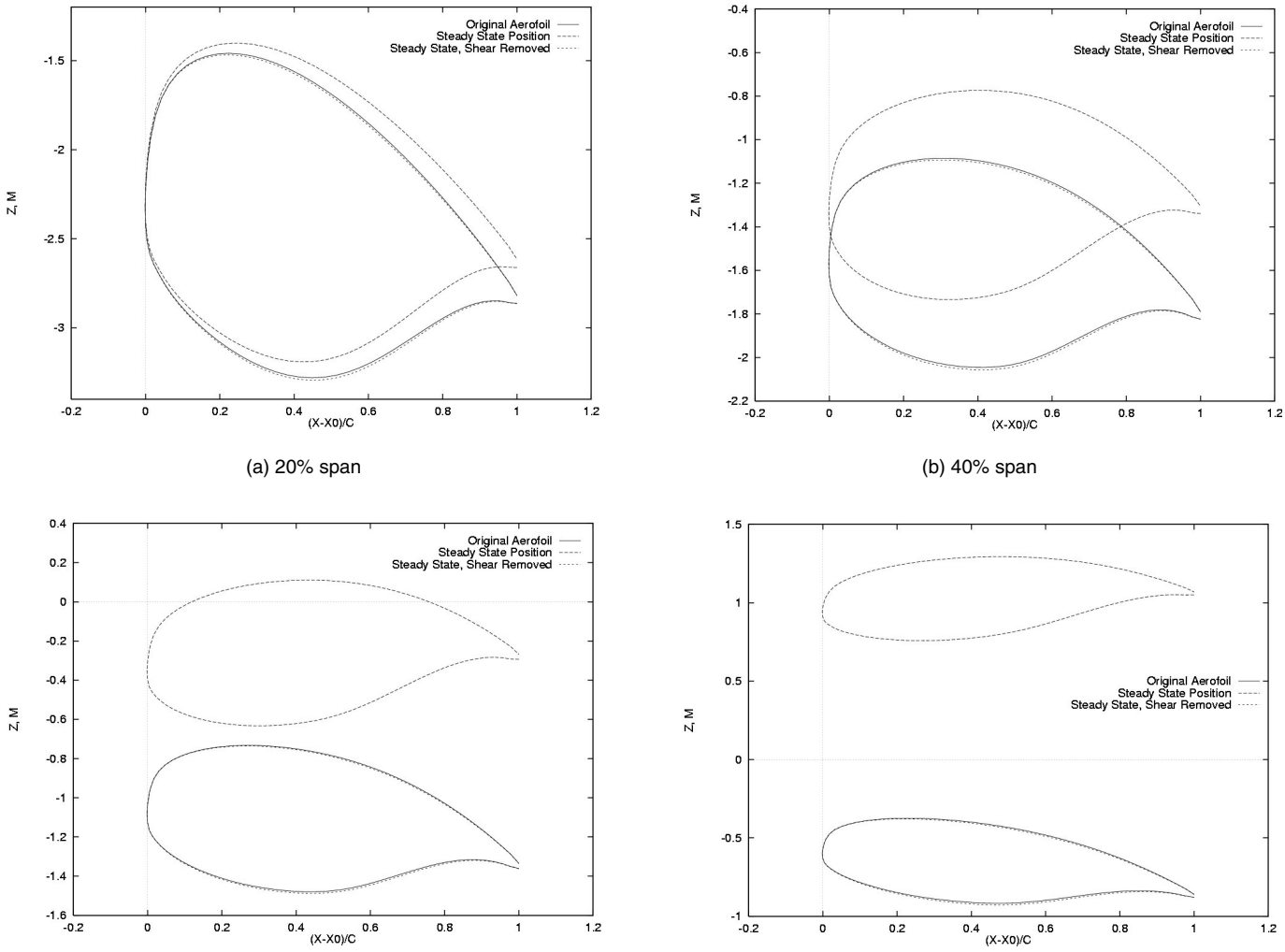
(b) trailing edge deformation

Figure 5. Wing distortion, MDO wing, Case 1, static load.

Figure 5 shows the relative displacement of the leading and trailing edge from their uncoupled position, where the span location is based upon the complete semi span of approximately 39m, rather than the exposed portion of approximately 35·5m. Agreement with the UNSI partners is excellent, despite the differences in incidence noted above.

The initial, steady state, and steady state with the structural shear removed aerofoil positions at 20, 40, 60 and 80% span are shown in

https://doi.org/10.1017/S0001924000000208 Published online by Cambridge University Press



(a) 20% span

(b) 40% span

(c) 60% span

(d) 80% span

Figure 6. Aerofoil distortions, MDO wing, steady state, Case 1.

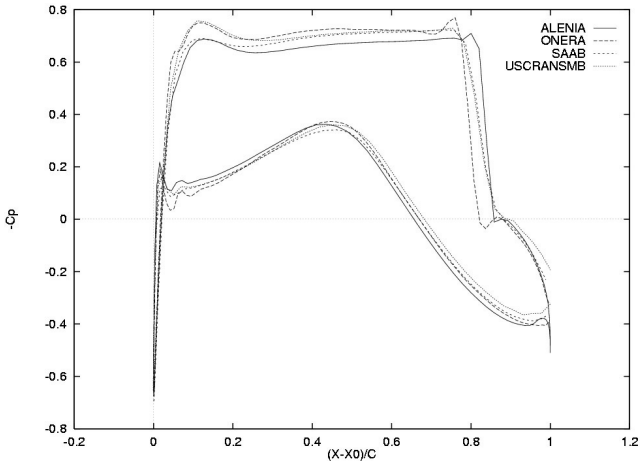
Fig. 6, and demonstrate that the interpolation is accurately preserving the aerofoil shape. Pressure distributions are compared in Fig. 7, for the same four spanwise stations. In general, the surface distributions are similar. In particular the shock wave position is in excellent agreement with the SAAB results, which use the most similar methodology, although it is noticeable that the forebody pressures are generally nearer the ONERA results. It is also clear that agreement between all methods is least impressive in the tip region.

4.2.2 Case 2

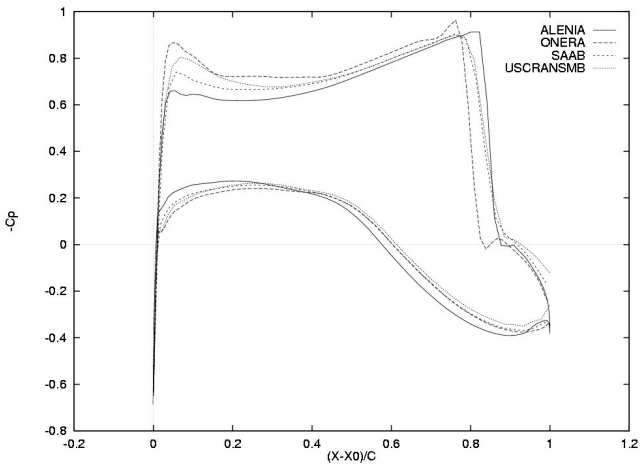
The desired lift coefficient of 0·3263 for Case 2 was produced by an incidence of 0·538 degrees, compared to SAAB and ONERA generated values of 0·248 and 0·439 degrees. Leading edge and trailing edge deflections are presented in Fig. 8, and again match the other Euler based solution methods well, particularly those of SAAB. The aerofoil sections are presented in Fig. 9, and demonstrate that the interpolation method is operating effectively. The pressure distributions at the specified spanwise locations show general agreement (Fig. 10), although the tendency for USCRANSMB to match SAAB shock wave position but ONERA forebody is still present (particularly for the inner portion of the wing), and once again tip results show a lesser corollary.

The time history of the wing tip deflection about the initial position produced by the unsteady calculation is shown in Fig. 11, compared to that produced by ONERA, for leading and trailing edge tip points. The agreement is good, given that the initial steady state positions differ slightly due to the different angle of attacks (and hence wing deflections) required for the designated lift coefficient. Apart from this mean discrepancy, the magnitudes and frequencies of the oscillations are in close agreement, although a higher degree of (aerodynamic) damping is present in the USCRANSMB analysis. Although numerical data for the Saab results were not available, the figures presented in Refs 15 and 16 qualitatively demonstrate that the general trend present in static test cases (that the USCRANSMB results lie somewhere between those of ONERA and Saab) is continued in the dynamic case, in that the motion predicted is of similar magnitude and frequency, but of still higher damping.

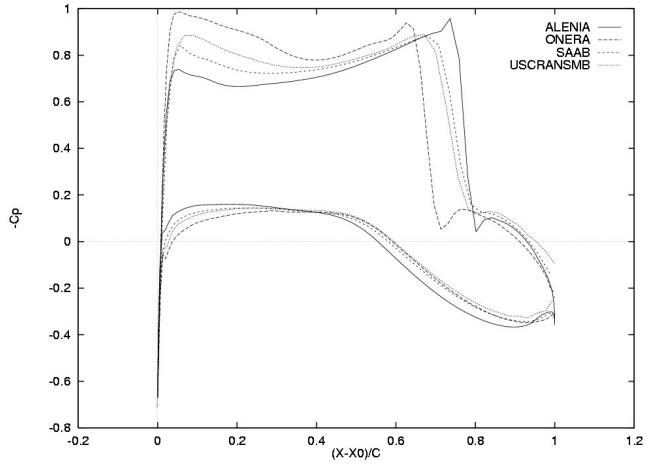
https://doi.org/10.1017/S0001924000000208 Published online by Cambridge University Press



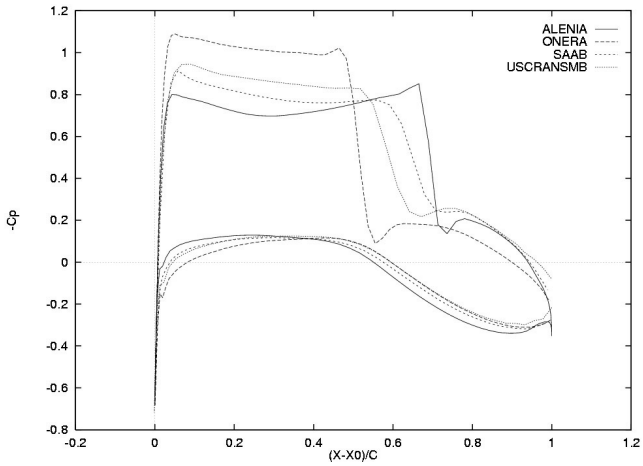
(a) 20% span



(b) 40% span

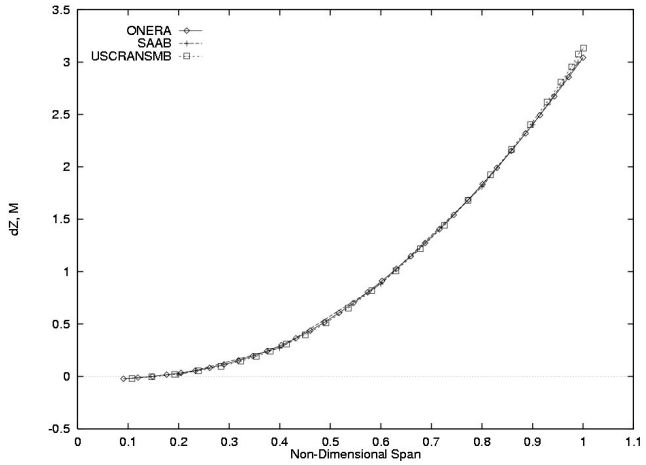


(c) 60% span

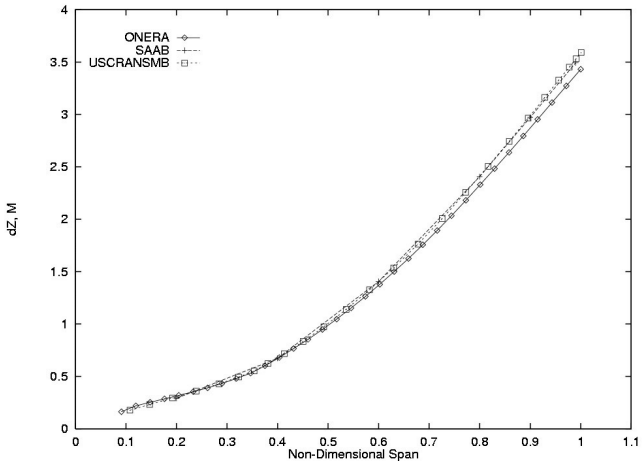


d) 80% span

Figure 7. Pressure distributions at various spanwise locations, MDO wing, Case 1.



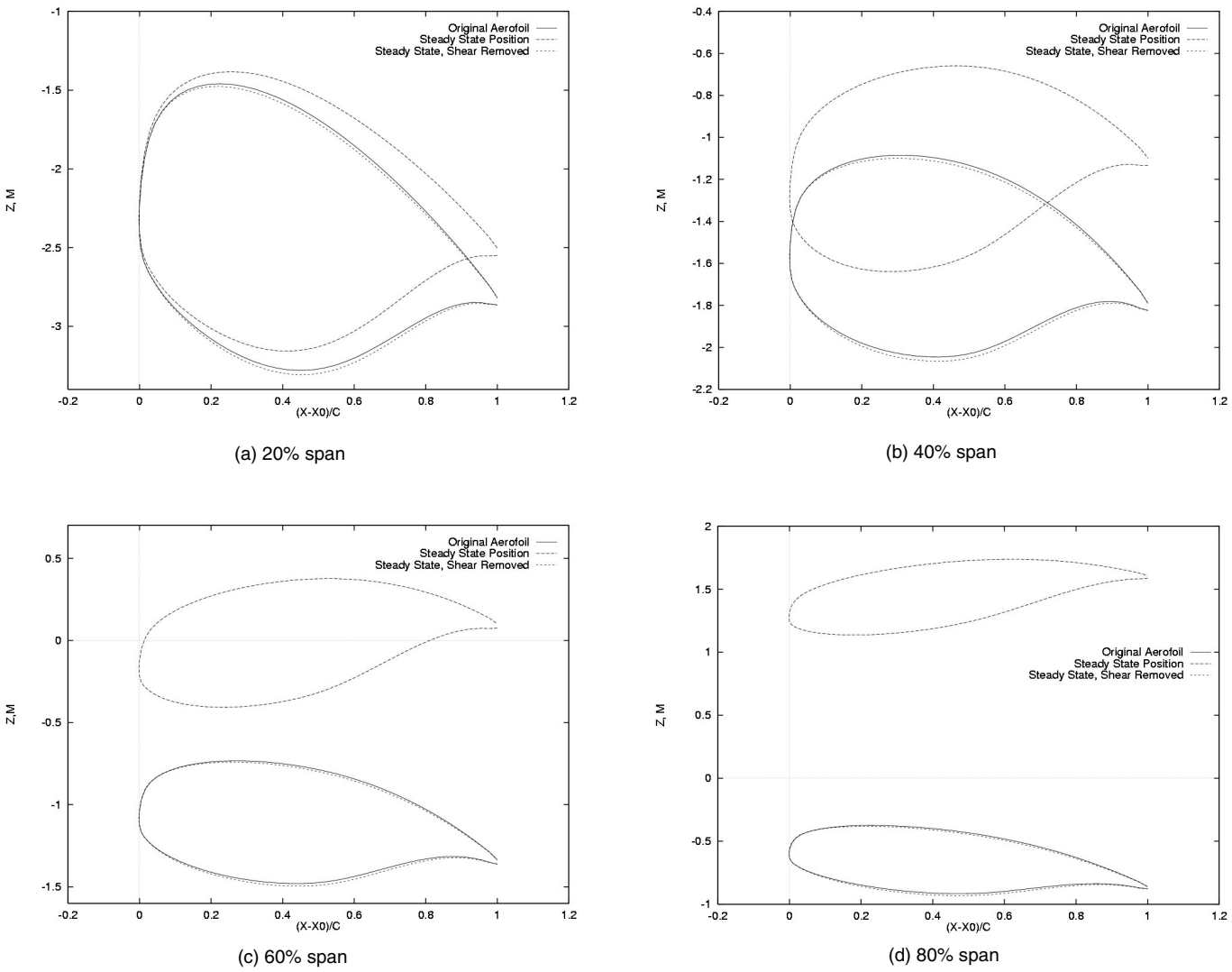
(a) leading edge deformation



(b) trailing edge deformation

Figure 8. Wing distortion, MDO wing, Case 2, static load.

https://doi.org/10.1017/S0001924000000208 Published online by Cambridge University Press



(a) 20% span

(b) 40% span

(c) 60% span

(d) 80% span

Figure 9. Aerofoil distortions, MDO wing, steady state, Case 2.

4.2.3 Case 3

The third test case presents the wing with aerodynamic conditions that result in unstable behaviour. An angle of incidence of –0·338 degrees produced the desired lift coefficient of 0·1685, compared to –0·649 and –0·404 for SAAB and ONERA respectively. The leading and trailing edge displacements (Fig. 12) are again similar to the other workers, although the difference in this case is more noticeable than Cases 1 and 2. The USCRANSMB generated results lie below ONERA and above SAAB, although nearer the latter. The aerofoil shape preservation (Fig. 13) remains accurate.

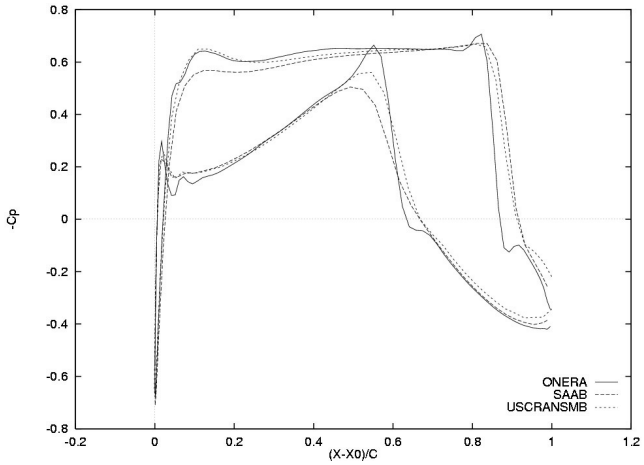
The dynamic response at the tip following the modal excitation is in excellent agreement with ONERA's results (Fig. 15), given the slight variation in initial deflection in the static case noted above.

4.3 Discussion

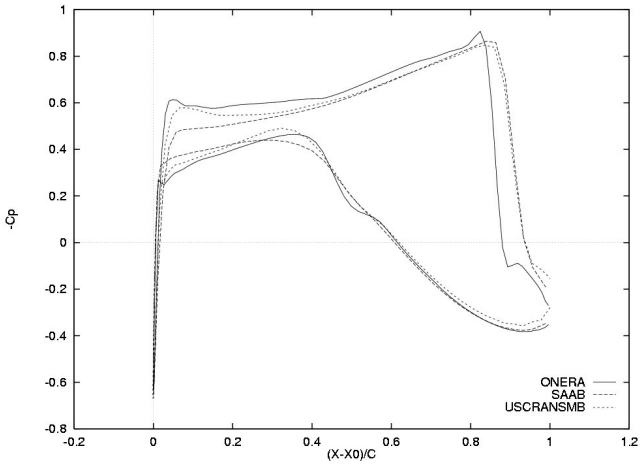
In all three test cases, the incidence predicted as being required to achieve a given lift coefficient was highest for USCRANSMB, and lowest for Saab. The wing deflections calculated using USCRANSMB have greatest similarity with the results produced by the deforming mesh method of Saab, as do the shock wave locations. However, forebody pressure distributions display better agreement with the transpiration method of ONERA, as do the dynamic responses (comparison of dynamic results with Saab unfortunately may only be achieved through visual inspection of the results given in Refs 15 and 16, but the differences are significant enough for this conclusion to be justified).

In general, it appears that the location of the shock wave is most

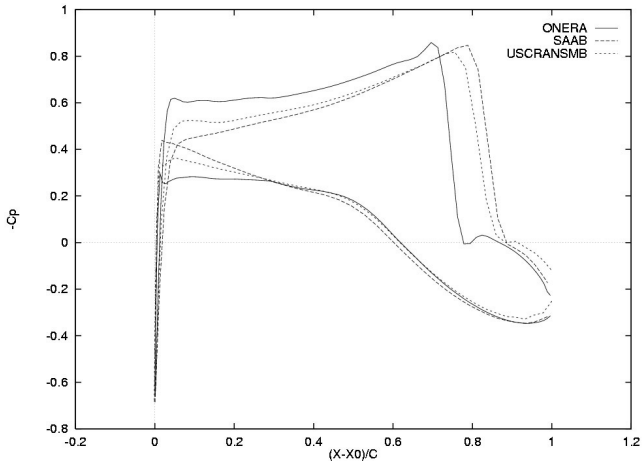
https://doi.org/10.1017/S0001924000000208 Published online by Cambridge University Press



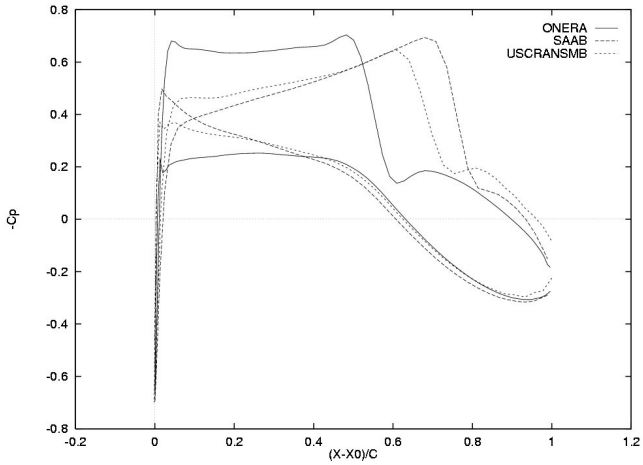
(a) 20% span



(b) 40% span

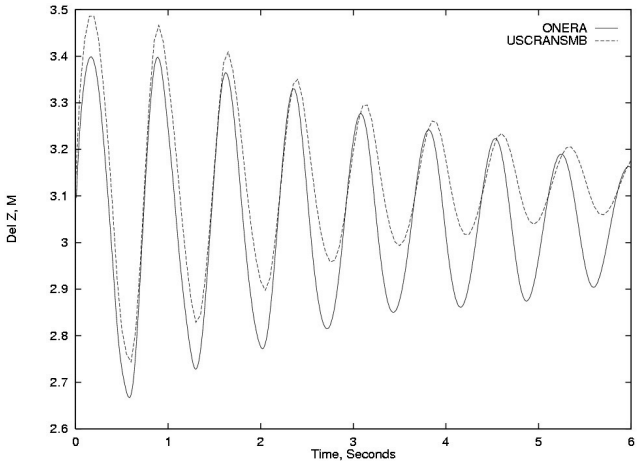


(c) 60% span

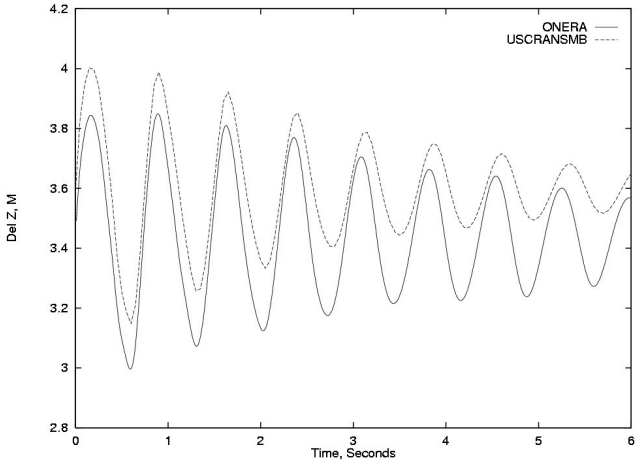


(d) 80% span

Figure 10. Pressure distributions at various spanwise locations, MDO wing, Case 2.



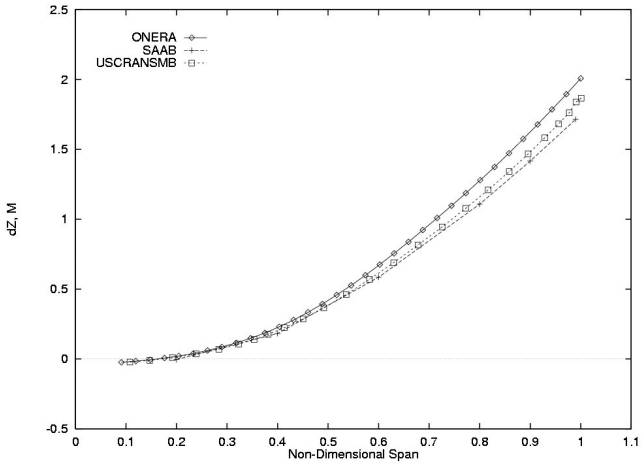
(a) leading edge deformation



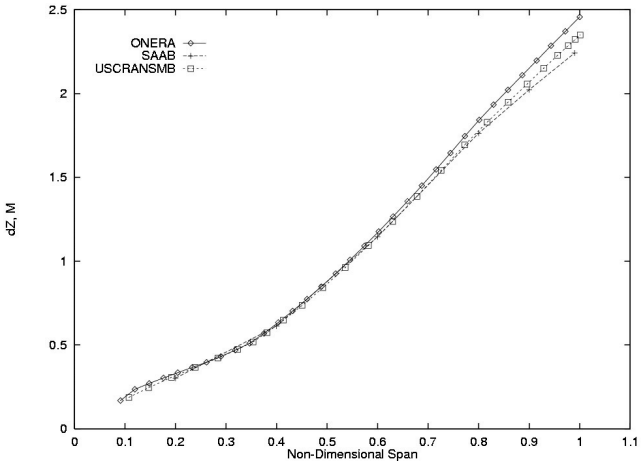
(b) trailing edge deformation

Figure 11. Dynamic response, MDO wing tip, Case 2.

https://doi.org/10.1017/S0001924000000208 Published online by Cambridge University Press

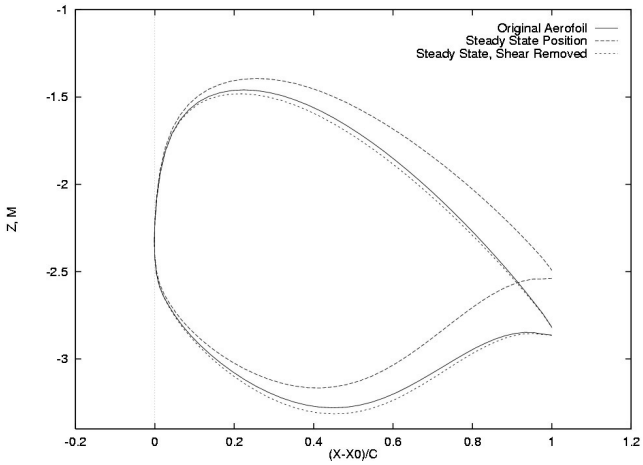


(a) leading edge deformation

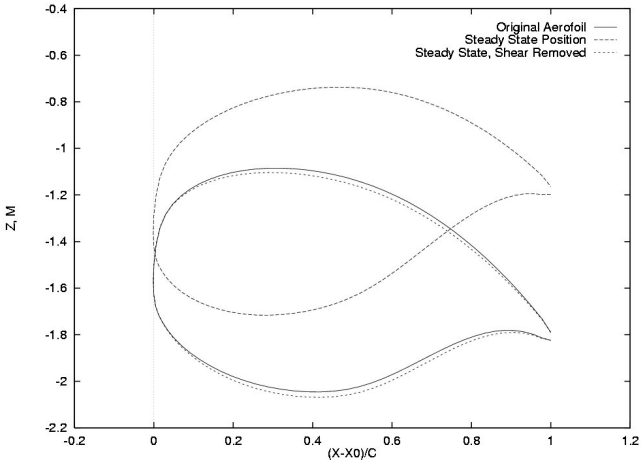


(b) trailing edge deformation

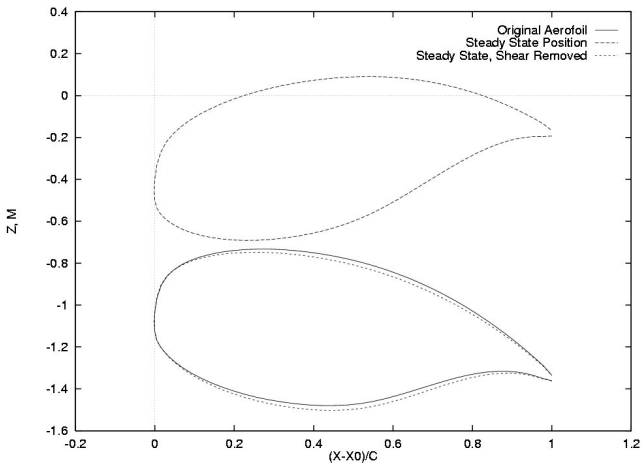
Figure 12. Wing distortion, MDO wing, Case 3, static load.



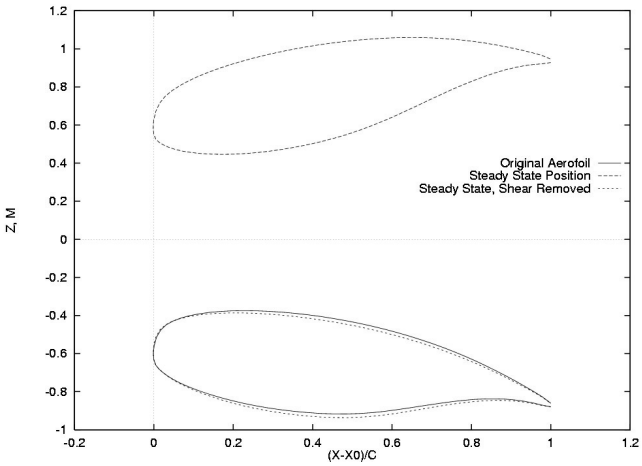
(a) 20% span



(b) 40% span



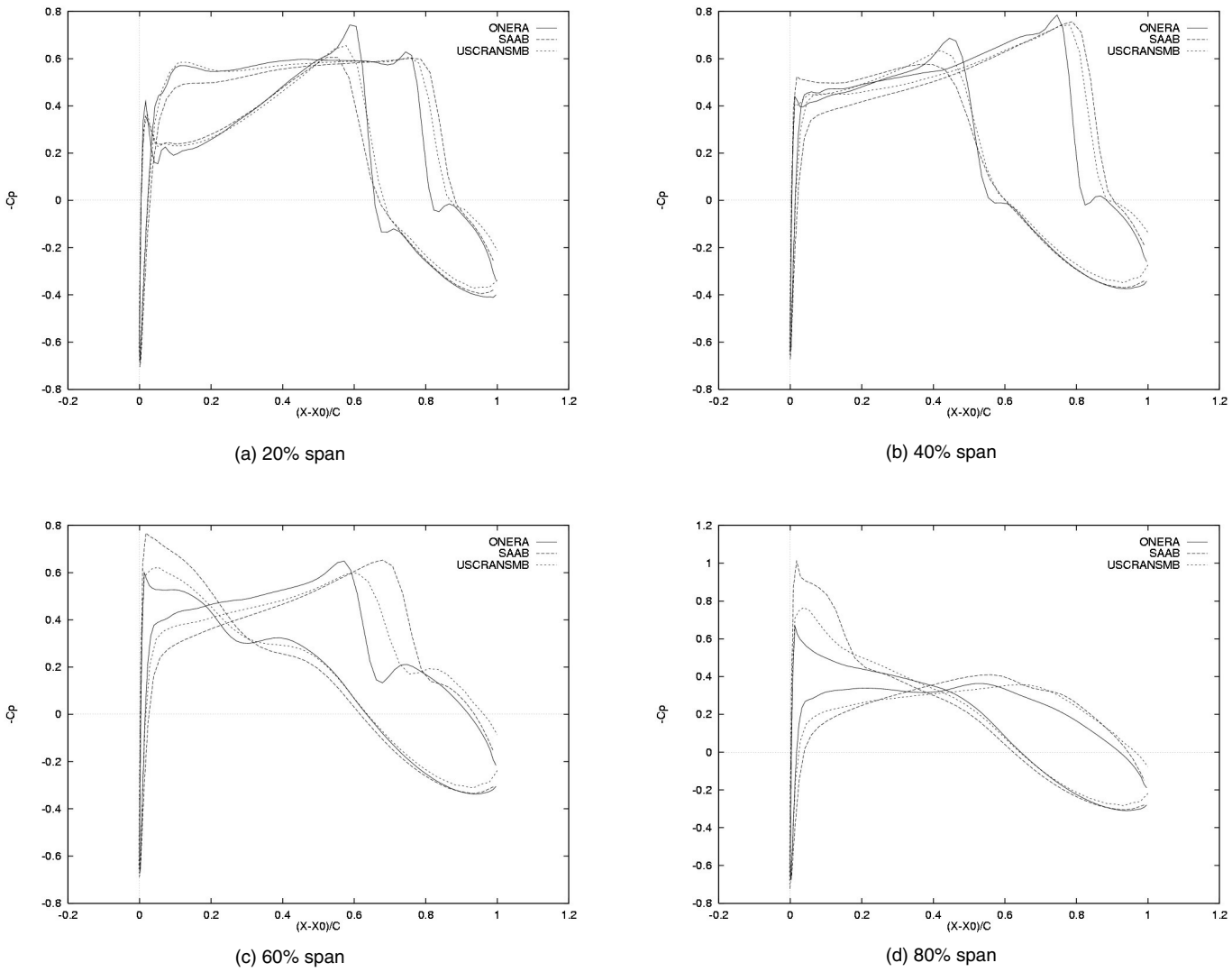
(c) 60% span



(d) 80% span

Figure 13. Aerofoil distortions, MDO wing, steady state, Case 3.

https://doi.org/10.1017/S0001924000000208 Published online by Cambridge University Press



(a) 20% span

(b) 40% span

(c) 60% span

(d) 80% span

Figure 14. Pressure distributions at various spanwise locations, MDO wing, Case 3.

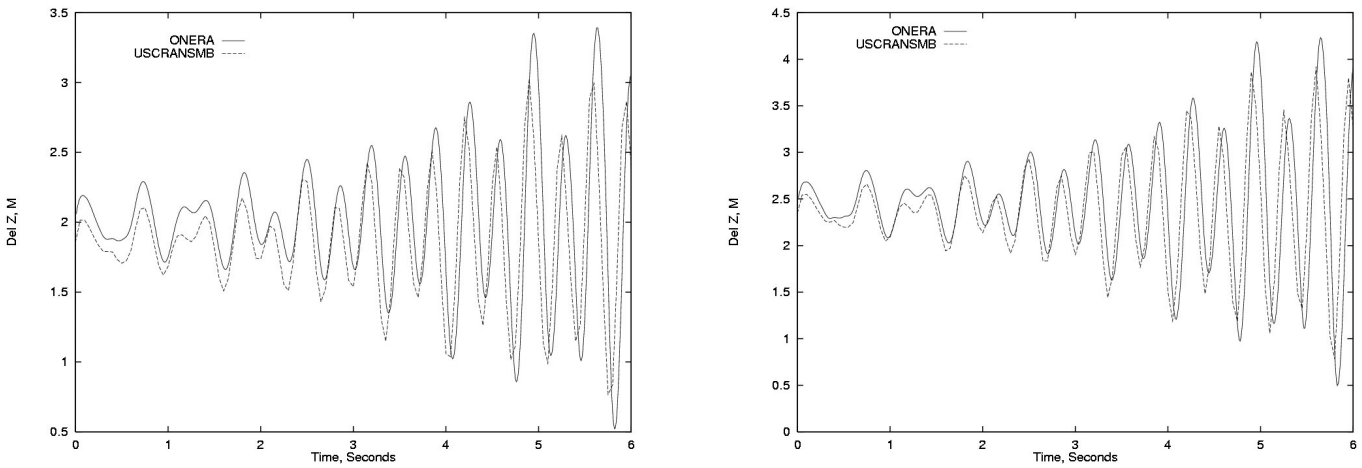
affected by the method used for surface motion, the transpiration results (ONERA) lying ahead of the predicted position of the two moving mesh codes (Saab and USCRANSMB). It is probable that as the shock lies within the region covered by the main structural mesh, the affect on its exact location of the interpolation method is lessened, as the two grids are nearly coincident here. However, it should also be noted that the shock position is likely to be influenced by the trailing edge deformations, which lie outside the range of the structural grid, and hence are more dependent on interpolation method.

Forebody pressure distributions demonstrate a higher degree of dependence on interpolation, as this region lies ahead of the leading edge of the structural grid. The similarity between the ONERA and USCRANSMB results in this region, particularly considering the greater aerodynamic grid density of the former, and the accuracy of shape preservation demonstrated by the latter, implies that these are the more accurate results. However, both these codes employ cell-centred differencing rather than the upwind code used by Saab, and this may also be partly responsible.

5.0 CONCLUSIONS

A time-accurate non-linear method for solution of aeroelastic flows based on coupled Euler-Modal analysis has been demonstrated and validated on two well known test cases. Further to this, the structural-aerodynamic grid interpolation has been demonstrated to main-

https://doi.org/10.1017/S0001924000000208 Published online by Cambridge University Press



(a) leading edge deformation

(b) trailing edge deformation

Figure 15. Dynamic response, MDO wing tip, Case 3.

tain the shape of an aerofoil of complex geometry, even for relatively large motions (the largest examined here produce a vertical tip deflection of almost 10% span). This will allow future development of alternative structural models and aeroservoelastic codes capable of modelling control surface activity with a fully integrated control system to be initiated with confidence in the underlying method. Such techniques are necessary for the design and analysis of active control of such instabilities as wing flutter and unsteady manoeuvre analysis, and are currently ongoing within the Aerospace Department at the University of Bristol.

ACKNOWLEDGEMENTS

The authors would like to thank Airbus UK, the EPSRC, and DSTL for providing the funding for this work, Glasgow University for providing aerodynamic grids and modal results, and Dr Graham Hill of the University of Bristol for his invaluable assistance with the fundamentals of structural analysis.

REFERENCES

1. KOUSED, K.A. and BENDIKSEN, O.O. Non-linear aspects of the transonic aeroelastic stability problem, 1988, AIAA Paper 88-2306. Also in AIAA/ASME/ASCE/AHS 29th Structures, structural dynamics and materials conference.
2. KOUSEN, K.A. and BENDIKSEN, O.O. Limit cycle phenomena in computational transonic aeroelasticity, *J Aircr,* November-December 1994, **31**, (6), pp 1257-1263.
3. ALONSO, J.J. and JAMESON, A. Fully-implicit time-marching aeroelastic solutions, January 1994, AIAA Paper 94-0056.
4. GURUSWAMAMY, G.P. Unsteady aerodynamic and aeroelastic calculations for wings using Euler equations, *AIAA J*, March 1990, **28**, (3), pp 461-469.
5. ROBINSON, B.A., BATINA, J.T. and YANG, H.T. Aeroelastic analysis of wings using the Euler equations with a deforming mesh, *J Aircr*, November 1991, **28**, (11), pp 781-788.
6. MEIJER, J.J., HOUNJET, M.H.L., EUSSEN, B.J.G. and PRANANTA, B.B. Nlr-Tu delf experience in unsteady aerodynamics and aeroelastic simulaiton applications, March 1998, Technical Report 822, AGARD, *Numerical Unsteady Aerodynamics and Aeroelastic Simulation*, pp 11-1-11-21.
7. SCHULTZE, S. Transonic aeroelasric simulation of a flexible wing section, March 1998, Technical Report 822, AGARD, *Numerical Unsteady Aerodynamics and Aeroelastic Simulation*, pp 10-1-10-20.
8. GOURA, G.S.L., BADCOCK, K.J., WOODGATE, M.A. and RICHARDS, B.E. Implicit method for the time marching analysis of flutter, *Aeronaut J*, April 2001, **105**, (4), pp 199-214.
9. BENDISKSEN, O.O. and KOUSEN, K.A. Transonic flutter analysis using the Euler equations, 1987, AIAA Paper 87-0911-CP.
10. BATINA, J.Y. and YOUNG, T.Y. Application of transonic codes to aeroelastic modelling of airfoils including active controls, *J Aircr*, August 1984, **21**, (8), pp 623-630.
11. LEE-RAUSCH, E.M. and BATINA, J.T. Wing flutter boundary prediction using unsteady Euler aerodynamic method, *J Aircr*, March-April 1995, **32**, (2), pp 416-422.
12. STEPHENS, C.H., ARENA, A.S. and GUPTA, K.K. CFD-based aeroservoelastic predictions with comparisons to benchmark experimental data, AIAA Paper 99-0766.
13. SEDAGHAT, A., COOPER, J.E., WRIGHT, J.R. and LEUNG, A.Y.T. Curve fitting approach for transonic flutter prediction, *Aeronaut J*, September 2003, **107**, (1007), p 565-572.
14. KANDIL, O.A., MASSEY, S.J. and SHETA, E.F. Structural dynamics–CFD interaction for computation of vertical tail buffet, *Aeronaut J*, August/September 1996, **100**, (997), pp 297-303.
15. HAASE, W., SELMIN, V. and WINZELL, B. (Eds). Progress in Computational flow-structure interaction, 2003, Vol 81, *Notes on Numerical Fluid Mechanics and Multidisciplinary Design*. Springer-Verlag.
16. GIRODOUX-LAVGNE, P., GRISVAL, J.P., GUILLEMOT, S., HENSHAW, M., KARLSSON, A, SELMIN, V., SMITH, J., TEUPOOTAHITI, E. and WINZELL, B. Comparison of static and dynamic fluid-structure interaction solutions in the case of a highly flexible modern transport aircraft wing, *J Aerospace Sci and Tech*, 2003, **7**, pp 121-133.
17. SCHMIDT, W., JAMESON, A. and TURKEL, E. Numerical solutions of the Euler equations by finite volume methods using runge-kutta time stepping schemes, 1981, AIAA Paper 81-1259.
18. KROL, N. and JAIN, R.K. Solution of two dimensional Euler equations — experience with a finite volume code, October 1987, Technical Report DFVLR-FB 87-41, DLR.
19. JAMESON, A. Time dependent calculations using multigrid with applications to unsteady flows past airfoils and wings, AIAA Paper 91-1596.
20. GAITONDE, A.L. A dual-time method for the solution of the unsteady Euler equations, *Aeronaut J*, October 1994, **98**, (978), pp 283-291.
21. ALLEN, C.B. The reduction of numerical entropy generated by unsteady shockwaves, *Aeronaut J*, January 1997, **101**, (1001), pp 9-16.
22. BADCOCK, K.J., SIM, G. and RICHARDS, B.E. Aeroelastic studies using transonic flow CFD modelling, 1995, International Forum on Aeroelasticity and Structural Dynamics, June 1995, pp 81.1-18.12.
23. PRANANTA B.B., HOUNJET, M.H.L. and ZWAAN, R.J. Thin layer Navier-Stokes solver and its application for aeroelastic analysis of an airfoil in transonic flow, 1995, International Forum on Aeroelasticity and Structural Dynamics , pp 1.1-1.9, June 1995.

https://doi.org/10.1017/S0001924000000208 Published online by Cambridge University Press

24. PRANANTA, B.B. and HOUNJET, M.H.L. Aeroelastic simulation with advanced CFD methods in 2-D and 3-D transonic flow, 1996, RAeS Symposium on Unsteady Aerodynamics, 17-18 July 1996, London, UK.
25. SCHULSTER, D.M., BERAN, P.S. and HUTTSELL, L.J. Applications of the en3dae euler/navier-stokes aeroelastic method, 1998, Technical Report 822, AGARD. *Numerical Unsteady Aerodynamic and Aeroelastic Simulations*, March 1998, pp 3-1-3-11.
26. VLACHOS, N. Aero-structural coupling in transonic flow: comparison of strong and weak coupling schemes, May 1999, Report DERA/ASF/3662U - AERO.RK5615.
27. DJAYAPERTAPA, L. A Computational Method for Coupled Aerodynamic-Structural Calculations in Unsteady Transonic Flow with Active Control Study, 2001, PhD thesis, Aerospace Engineering Department, Bristol University.
28. GERADIN, M. and RIXEN, D. *Mechanical Vibrations*, 1997, Second edition, John Wiley and Sons, Chichester, UK.
29. BATHE, K.J. *Finite Element Procedures in Engineering Analysis*, 1982, Prentice Hall, Englewood Cliffs. New Jersey, USA.
30. APPA, K., YANKULICH, M. and COWAN, D.L. The determination of load and slope transformation matrices for aeroelastic analysis, *J Aircr*, 1985, **22**, pp 734-736.
31. APPA, K. Finite surface splines, *J Aircr*, 1989, **26**, pp 495-496.
32. GURUSWAMY, G.P. A review of numerical fluids/structures interface methods for computations using high-fidelity equations, *Computers and Structures*, 2002, **80**, pp 31-41.
33. GOURA, G.S.L. Time Marching Analysis of Flutter using Computational Fluid Dynamics, 2001, PhD thesis, Department of Aerospace Engineering, Glasgow University.
34. GOURA, G.S.L., BADCOCK, K.J., WOODGATE M.A. and RICHARDS, B.E. A data exchange method for fluid-structure intraction problems, *Aeronaut J*, April 2001, **105**, (4), pp 215-221.
35. DUCHON, J. Splines minimising rotation-invariant semi-norms in Sobolev spaces, *Constructive Theory of Functions of Several Variables*, 1976, Springer (Germany).
36. MADYCH, W.R. and NELSON, S.A. Multivariate interpolation: a variational theory, *J Approx Theory Applic*, 1990.
37. SMITH, M.J. HODGES, D.H. and CESNIK, C.E.S. Evaluation of computational algorithms to interface for fluid structure interaction, *J Aircr*, 2000, **37**, (2), pp 282-295.
38. FRANK, R. Scattered data interpolation: test of some methods, *Mathematics of Computations*, 1982, **38**, pp 181-199,.
39. JONES, D.P. Force transfer in aeroelastic calculations, December 2002, Technical Report AE047, University of Bristol.
40. JONES, D.P. Interpolation method in CFD-CSD calculations, 2004, in preparation.
41. YATES, E.C. Standard aeroelastic configurations for dynamic response i-wing 445.6, September 1985, Technical Report 765 AGARD, includes Tech Report Tn-D-1616 as an Appendix.
42. YATES, E.C., LAND, N.S. and FOUGHNER, J.T. Measured and calculated subsonic and transonic flutter characteristics of a 45 deg sweptback wing platform in air and in Freon-12 in the Langley transonic dynamics tunnel, March 1963, Technical Report Tn-D-1616, NASA.
43. TAYLOR N.V. Unsteady aerodynamic simulation by flight control system integration with structure-coupled CFD, November 2003, Technical Report AE046, University of Bristol.
44. ALLEN, C.B., FENWICK, C.L., TAYLOR N.V. and DJAYAPERTAPA, L. Investigation of flutter suppresion by active control, 2003, AIAA Paper 2003-3510, 21st AIAA Applied Aerodynamics Conference, Florida, June 2003.
45. GOURA, G.S.L., BADCOCK, K.J., WOODGATE, M.A. and RICHARDS, B.E. Notes on MDO test case, unpublished report supplied by Glasgow University.

https://doi.org/10.1017/S0001924000000208 Published online by Cambridge University Press